Int. J. Heat Mass Transfer. Vol. 33, No. 9, pp. 1805–1816, 1990
Printed in Great Britain

0017-9310/90 $3.00 + 0.00

Laminar mixed convection in a radially rotating semiporous channel

C. Y. SOONG† and G. J. HWANG‡
Department of Power Mechanical Engineering, National Tsing Hua University, Hsinchu, Taiwan 30043, R.O.C.

(*Received* 17 *July* 1989 *and in final form* 6 *October* 1989)

Abstract—Flow and heat transfer characteristics of laminar mixed convection in a radially rotating semiporous channel with a uniform transpiration and a constant wall temperature gradient are examined. The buoyancy effect is taken into account through the consideration of the density variation in the centrifugal force term. A similarity solution is sought; and then the effects of rotation, transpiration and wall heating on the velocity and temperature fields, the skin friction, the pressure drop and the heat transfer rate are investigated by the solution of the two coupled quasilinear equations. Flow-reversal phenomena can be caused by the transpiration and buoyancy effects. Two modes of flow reversal and the related critical conditions are studied in detail to explore the mechanism of the mixed convection.

INTRODUCTION

THE FLUID flow and heat transfer in porous-walled flow passages have received a great deal of attention in the past decades due to their wide application in a variety of thermal systems such as gas-turbine rotor blades, combustion chambers, exhaust nozzles, porous-walled flow reactors and solar energy systems. The theoretical study may be traced back to Berman's similarity solution [1] for the incompressible laminar fully-developed flow in a two-dimensional fully porous-walled channel (FPC) with a uniform transpiration. Later, Yuan and Finkelstein [2] developed the counterpart similarity solution for flow in a porous-walled tube. Since then, the research in this area has become vital. The corresponding heat transfer characteristics were also investigated extensively [3–6]. Among these investigations, Carter and Gill's work [3] is noteworthy. The similarity equations for mixed convection in vertical and horizontal FPCs and porous-walled tubes were proposed and solved by using methods of weighted residuals. Suction and injection were considered, but only the solutions with a small wall suction ($Re_w \leqslant 1$) were obtained due to the limitation of the method they used.

Flow and heat transfer characteristics in the semiporous channel (SPC) are somewhat different from those in the FPC. The former case has been studied only in a few previous works. Donoughe [7] and Eckert *et al.* [8] solved Berman's equation for fluid flow in SPC. Heat transfer in the hydrodynamic and thermal entrance region of SPC with a tail-end-plate was first examined numerically by Rhee and Edwards [9]. Later, Sorour and Hassab [10] used the solution of Berman's equation to recast the energy equation into an eigenvalue problem which was then solved numerically. More recently, Sorour *et al.* [11] reconsidered Rhee–Edward's flow configuration with a linearly varying transpiration velocity.

At an engineering standpoint, the transpiration cooling in the turbine rotor blades can be modelled as the mixed convection in a radially rotating SPC. Rotation of the channel may generate significant effects on the flow and temperature fields. To the authors' best knowledge, however, the mixed convection in the radially rotating porous channels has not been reported in the literature yet. The typical transpiration cooling channel in turbine blades is of low height and width aspect ratio as those used in the engine tests [12, 13]. Therefore, to gain insight into the fundamental nature of this complex flow field, a two-dimensional mixed convection analysis in a radially rotating semiporous channel is proposed for the problem. Both the case of radially outward and inward main flows are studied; and the rotational effects, including the Coriolis and centrifugal-buoyancy forces, are considered. By assuming a large semispan eccentricity and slenderness of the channel, and imposing the thermal boundary condition of a constant wall temperature gradient, the similarity equations are derived and then solved to examine the effects of rotation, transpiration and wall heating on the velocity and temperature fields, the skin friction, the pressure drop and the heat transfer rate. A closed-form analytic solution is found readily when wall transpiration is absent. Flow reversal may be induced by wall-transpiration and buoyancy effects. The critical conditions for the threshold of the flow reversal are studied in various combinations of the transpiration and wall heating parameters.

† Present address: Department of Aeronautical Engineering, Chung Cheng Institute of Technology, Taoyuan, Taiwan 33509, R.O.C.
‡ Author to whom correspondence should be addressed.

NOMENCLATURE

C_f skin friction coefficient
E semispan eccentricity
f dimensionless stream function or transverse velocity, V/V_w
g dimensionless temperature, $(T-T_{sw})/(Pe\cdot\Delta T_c u_m)$
H channel height
h heat transfer coefficient
k thermal conductivity
L channel length
Nu Nusselt number, hH/k
P static pressure
$\tilde{P}$ reduced pressure, $P+(\rho\omega^2/2)[(X\pm X_0)^2+Y^2]$
P', p' dimensional and dimensionless pressure departure, $p'=P'/\rho_r U_0^2$
Pe Peclet number, $Pr\,Re$
Pr Prandtl number, ν/α
$\mathbf{R}$ position vector emanating from rotation centre
Ra_ω rotational Rayleigh number, $(X_c\omega^2\beta\Delta T_c H^3\,Pr)/\nu^2$
Re main flow Reynolds number, U_0H/ν
Re_w wall suction Reynolds number, V_wH/ν
Ro rotation number, $\omega H/U_0$
T temperature
ΔT_c characteristic temperature difference, τH
U, V velocity components
U_0 mean velocity at $X=0$
U_m mean velocity at axial location X, $U_m=U_m(X)$
u, v dimensionless velocity components, U/U_0 and V/U_0
X, Y coordinates
x, y dimensionless coordinates, X/H and Y/H.

Greek symbols
α thermal diffusivity
β thermal expansion coefficient
δ dimensionless wall temperature difference, $(T_{pw}-T_{sw})/(Pe\,\Delta T_c u_m)$
ε dimensionless semispan eccentricity, E/H
θ dimensionless temperature difference, $(T-T_r)/\Delta T_c$
μ viscosity
ν kinematic viscosity
Π pressure-drop parameter, $\int_0^1[(-Re_x/\rho U_m^2)(\partial\tilde{P}/\partial x)+2Ro\,Re_w(U_0/U_m)f]\,dy$
ρ density
τ solid wall temperature gradient
Ψ stream function
ω rotational speed.

Subscripts
cr critical condition
m mean
pw porous wall
r reference condition
sw solid wall
ω rotational condition.

THEORETICAL ANALYSIS

Flow configuration and basic equations

As shown in Fig. 1, a semiporous channel with solid and porous walls separated by a height H rotates at a speed ω about an axis perpendicular to the axis of the channel. The rotational axis lies at a distance X_0 away from the origin of the coordinate system which is fixed on the channel entrance. Fluid flows along the channel axis as well as bleeds out through the porous wall at a constant transpiration velocity V_w along the channel length. Two modes of main flow, radially outward and inward, are considered. The flow is assumed to be laminar and steady, and the compression work and the viscous dissipation are negligible. Since the buoyancy effect may be significant in the presence of the high centrifugal acceleration, Boussinesq's approximation is invoked to allow for a linear variation of density with temperature, in the centrifugal force term. The gravitational effect, in this problem, is comparatively small and can be neglected.

Subject to the above conditions, the conservation equations for mass, momentum and energy are depicted as follows [14]:

$$\nabla\cdot\mathbf{V}=0 \tag{1}$$

$$(\mathbf{V}\cdot\nabla)\mathbf{V}=\nu\nabla^2\mathbf{V}-\nabla P'/\rho_r+\beta(T-T_r)(\omega\times\omega\times\mathbf{R})-2\omega\times\mathbf{V} \tag{2}$$

$$(\mathbf{V}\cdot\nabla)T=\alpha\nabla^2T \tag{3}$$

where $P'=P-P_r$ is the pressure departure from the reference condition, subscript r denotes the condition at the origin (0, 0) and is used as the reference condition, and $\mathbf{R}$ the position vector emanating from the rotation centre. The governing equations can be writtten in dimensionless forms as

$$\frac{\partial u}{\partial x}+\frac{\partial v}{\partial y}=0 \tag{4}$$

$$u\frac{\partial u}{\partial x}+v\frac{\partial u}{\partial y}=\frac{1}{Re}\nabla^2u-\frac{\partial p'}{\partial x}-\frac{Ra_\omega}{Pe\,Re}\left(\frac{x\pm x_0}{x_c}\right)\theta+2Ro\cdot v \tag{5}$$

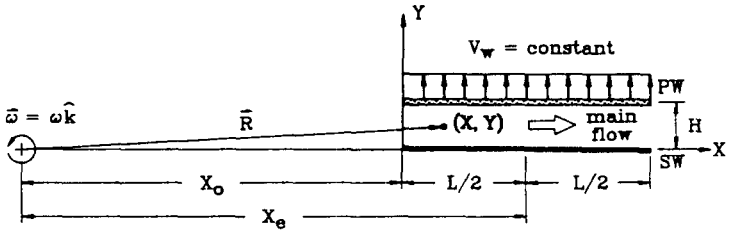

(a) Radially outward flow, $\vec{R} = (X + X_o)\hat{i} + Y\hat{j}$

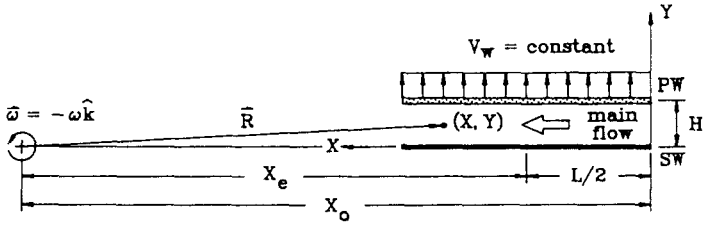

(b) Radially inward flow, $\vec{R} = (X - X_o)\hat{i} + Y\hat{j}$

FIG. 1. Flow configurations and coordinate system: PW, porous wall; SW, solid wall.

$$u\frac{\partial v}{\partial x} + v\frac{\partial v}{\partial y} = \frac{1}{Re}\nabla^2 v - \frac{\partial p'}{\partial y} - \frac{Ra_\omega}{Pe\,Re}\left(\frac{y}{x_e}\right)\theta - 2Ro\cdot u \quad (6)$$

$$u\frac{\partial \theta}{\partial x} + v\frac{\partial \theta}{\partial y} = \frac{1}{Pe}\nabla^2\theta. \quad (7)$$

The reference velocity U_0 used is the mean velocity at $X = 0$, $T_r = T_{sw}(0)$ is the solid-wall temperature at $X = 0$ and ΔT_e is the characteristic temperature difference to be determined later. The two non-dimensional groups, the rotation number Ro and the rotational Rayleigh number Ra_ω, characterize the Coriolis force and the centrifugal-buoyancy effects, respectively. On the right-hand side of equation (5), the upper plus sign in the buoyancy term is taken if the main flow is radially outward and the lower minus sign if the flow is radially inward.

The boundary conditions on the solid and porous walls are $u = v = 0$ and $\theta = \theta_{sw}(x)$ at $y = 0$; and $u = v - v_w = 0$ and $\theta = \theta_{pw}(x)$ at $y = 1$. The subscripts sw and pw denote the solid wall and the porous wall, respectively.

Similarity transformation

To achieve a similarity solution for the above governing equations, the proper invariant profile functions must be found. Since the fluid is substracted through the porous wall at the rate of ρV_w per unit length, the local mean velocity along the channel length is thus $U_m(X) = U_0 - V_w X/H$ or in a dimensionless form $u_m(x) = 1 - v_w x$. Following Berman's original proposal for the fully-developed flow, the stream function is defined as

$$\Psi(x, y) = u_m(x)\cdot f(y). \quad (8)$$

By defining $u = \partial\Psi/\partial y$ and $v = -\partial\Psi/\partial x$, one has

$$u/u_m = f'(y) \quad \text{and} \quad v/v_w = f(y). \quad (9)$$

Note that equations (9) satisfy continuity equation (4) automatically. Eliminating the pressure terms in the momentum equations (5) and (6) by a cross differentiation and using equations (9), one has the resultant equation of motion

$$f^{iv} - Re_w(ff''' - f'f'') = \frac{Ra_\omega}{Pe\cdot u_m}\left(\frac{x \pm x_0}{x_e}\frac{\partial\theta}{\partial y} - \frac{y}{x_e}\frac{\partial\theta}{\partial x}\right) \quad (10)$$

where $Re_w = V_w H/\nu$ is the wall Reynolds number which characterizes the effect of wall transpiration.

To simplify the analysis, two approximations are employed. First, the channel length is sufficiently small as compared with the semispan eccentricity [15]. This leads to simplifications $(X \pm X_0)/X_e \cong \pm 1$ and $\omega^2(X \pm X_0) \cong \pm\omega^2 X_e$. Second, the coolant channel is very slender, $Y/X_e \ll 1$, and also has $\partial\theta/\partial y \gg \partial\theta/\partial x$. Consequently, the last term in equation (10) can be ignored.

Two situations, the buoyancy-opposed mixed convection with $Ra_\omega(x \pm x_0)/x_e > 0$ and buoyancy-assisted one with $Ra_\omega(x \pm x_0)/x_e < 0$ are considered. To unify the equation of motion, the sign of $(x \pm x_0)/x_e$ can be absorbed into the parameter Ra_ω. The positive Ra_ω is responsible for the case of buoyancy-opposed flow and the negative Ra_ω stands for the case of buoyancy-assisted flow. Finally, equation (10) reduces to

$$f^{iv} - Re_w (ff''' - f'f'') = \frac{Ra_\omega}{Pe \cdot u_m} \frac{\partial \theta}{\partial y}. \quad (11)$$

Equation (11) implies that the similarity form exists if $\theta(x, y)$ is of the form

$$\theta(x, y) = \theta_{sw}(x) + Pe \cdot u_m(x) \cdot g(y). \quad (12)$$

Substituting equation (12) into the energy equation (7), one obtains

$$g'' - Pr\, Re_w (fg' - f'g) = \frac{T'_{sw}(x)}{\Delta T_c} \cdot f' - \frac{T''_{sw}(x)}{Pe \cdot u_m(x) \cdot \Delta T_c}. \quad (13)$$

To attain the similarity, $T_{sw}(x)$ must be linear in x and, for convenience, it is specified as $T_{sw}(x) = T_{sw}(0) + \Delta T_c x$. The characteristic temperature difference can now be determined at $\Delta T_c = \tau H$, in which τ is the slope of the prescribed solid-wall temperature. By defining $g(1) = \delta$, the porous-wall temperature $T_{pw}(x)$ can also be expressed in a linear form. The parameter δ represents the temperature difference between the solid and the porous walls; and therefore, it is also an index of asymmetry of the wall heating.

Finally, by using the similarity variables $f(y)$ and $g(y)$ and imposing different constant temperature gradients to the walls, the resultant similarity equations are

$$f^{iv} - Re_w (ff''' - f'f'') = Ra_\omega \cdot g' \quad (14)$$

$$g'' - Pr\, Re_w (fg' - f'g) = f'. \quad (15)$$

The associated boundary conditions are

$$f(0) = f'(0) = f'(1) = f(1) - 1 = 0$$

$$g(0) = g(1) - \delta = 0. \quad (16)$$

Flow and heat transfer parameters

The general expression for the skin friction coefficient is defined as

$$C_f = 2\mu(\partial U/\partial Y)_w / \rho U_m^2(X). \quad (17)$$

Then, based on the velocity solution of the problem, the products of the friction coefficient and the Reynolds number for the solid and porous walls are

$$C_{f,sw}\, Re_x = 2f''(0) \quad (18)$$

and

$$C_{f,pw}\, Re_x = -2f''(1) \quad (19)$$

respectively. Re_x is the Reynolds number based on the local mean velocity, $U_m H/\nu$.

The pressure-drop parameter Π is defined as the cross-sectional average of

$$-\frac{Re_x}{\rho U_m^2}\left(\frac{\partial \tilde{P}}{\partial x}\right) + 2Ro\, Re_w \left(\frac{U_0}{U_m}\right) f$$

wherein the contributions of the Coriolis and centrifugal forces have been involved, and

$$\Pi = -f'''(0) - Ra_\omega \int_0^1 g(y)\, dy \quad (20)$$

where

$$\tilde{P} = P + \frac{\rho\omega^2}{2}[(X + X_0)^2 + Y^2]$$

is the reduced pressure.

The heat transfer rate is characterized by the Nusselt number. From the heat balance at the wall, the Nusselt number can be defined as

$$Nu = hH/k = -(\partial T/\partial Y)_w / (T_w - T_b) \quad (21)$$

where

$$T_b(X) = \frac{1}{U_m H} \int_0^H UT\, dY$$

is the bulk temperature of the fluid. The resultant Nusselt numbers at solid and porous walls can be written as

$$Nu_{sw} = g'(0) \Big/ \int_0^1 f'g\, dy \quad (22)$$

and

$$Nu_{pw} = g'(1) \Big/ \left(\delta - \int_0^1 f'g\, dy\right). \quad (23)$$

In the case of $Re_w \neq 0$, the integral in equations (22) and (23) can be evaluated directly by integrating energy equation (15)

$$\int_0^1 f'g\, dy = \frac{\delta}{2} + \frac{1}{2Pr\, Re_w}[1 + g'(0) - g'(1)]. \quad (24)$$

When transpiration is absent, this integral can be evaluated simply by using the analytic solutions of zero transpiration.

ANALYTIC SOLUTIONS FOR ZERO TRANSPIRATION

Equations (14) and (15) with the associated boundary conditions (16) describing the present problem are coupled high-order quasi-linear differential equations. Exact analytic solution to this problem is almost impossible. The case of zero transpiration, i.e. $Re_w = 0$, however, removes the nonlinearity and highly simplifies the system. In this circumstance, one has

$$f^v - Ra_\omega f' = 0 \quad \text{or} \quad f^{iv} - Ra_\omega f = f^{iv}(0). \quad (25)$$

The corresponding five boundary conditions are

$$f(0) = f'(0) = f(1) - 1 = f''(1) = 0$$

and

$$f^{iv}(0) = Ra_\omega \left[\delta - \int_0^1 f(y)\, dy\right]. \quad (26)$$

Mathematically, the solutions are different in the cases of $Ra_\omega = 0$, >0 and <0 corresponding physically to the pure forced convection, the buoyancy-opposed and the buoyancy-assisted mixed convection, respectively. The closed-form solutions are found analytically as follows.

A. Forced convection ($Ra_\omega = 0$)

$$f(y) = 3y^2 - 2y^3 \tag{27}$$

$$g(y) = (\delta - \tfrac{1}{2})y + y^3 - \tfrac{1}{2}y^4. \tag{28}$$

This is the so-called Poiseuille-type flow.

B. Buoyancy-opposed mixed convection ($Ra_\omega > 0$)

$$f(y) = C_1 + C_2 \sinh Ky + C_3 \cosh Ky + C_4 \sin Ky + C_5 \cos Ky \tag{29}$$

$$g(y) = \delta y + \frac{1}{K}\{C_2[(\cosh Ky + \cos Ky) - y(\cosh K + \cos K) - 2(1-y)] + C_3(\sinh Ky - y\cdot\sinh K) + C_5(\sin Ky - y\cdot\sin K)\} \tag{30}$$

where

$$C_5 = \frac{1}{\Delta_1}\{2\sinh K(1-\cos K) - K\delta[\sin K\cdot\sinh K - (1+\cos K)(\cosh K - 1)]\}$$

$$C_4 = \frac{1}{\Delta_1}\{K\delta[\sinh K(\cos K - 1) + \sin K(\cosh K - 1)] - 2\sin K\sinh K\}$$

$$C_3 = C_4(\cosh K - \cos K)/\sinh K + C_5 \sin K/\sinh K$$

$$C_2 = -C_4; \quad C_1 = -C_3 - C_5$$

$$\Delta_1 = -4[\sinh K(1-\cos K) - \sin K(\cosh K - 1)]$$

$$K = Ra_\omega^{1/4}.$$

C. Buoyancy-assisted mixed convection ($Ra_\omega < 0$)

$$f(y) = \frac{f''(0)}{2a^2}\sin ay\cdot\sinh ay + \frac{f'''(0)}{4a^3}(\sin ay\cdot\cosh ay - \cos ay\cdot\sinh ay) + \frac{f^{iv}(0)}{4a^4}(1-\cos ay\cdot\cosh ay) \tag{31}$$

$$g(y) = \delta y - \frac{f''(0)}{4a^3}[\sin ay\cdot\cosh ay - \cos ay\cdot\sinh ay - y(k_2 - k_3)] - \frac{f'''(0)}{4a^4}[1 - \cos ay\cdot\cosh ay - y(1-k_4)] + \frac{f^{iv}(0)}{8a^5}[\sin ay\cdot\cosh ay - \cos ay\cdot\sinh ay - y(k_2 + k_3)] \tag{32}$$

where

$$f''(0) = \frac{1}{\Delta_2}[8a^6\delta(k_2 - k_3)^2 - 8a^5k_1(k_2 + k_3) - 8a^5(1-k_4)(k_2 - k_3) - 16a^6\delta k_1(1-k_4)]$$

$$f'''(0) = \frac{1}{\Delta_2}[8a^6(k_2 - k_3)^2 + 16a^7\delta(1-k_4)(k_2 + k_3) + 8a^6(k_2 + k_3)^2 - 16a^7\delta k_1(k_2 - k_3)]$$

$$f^{iv}(0) = \frac{1}{\Delta_2}[16a^7(1-k_4)(k_2 + k_3) + 32a^8\delta k_1^2 - 16a^8\delta(k_2^2 - k_3^2) - 16a^7k_1(k_2 - k_3)]$$

$$\Delta_2 = 2a^3(k_2 - k_3)^3 + 4a^3(1-k_4)^2(k_2 + k_3) - 4a^3k_1^2(k_2 + k_3) + 2a^3(k_2 + k_3)(k_2^2 - k_3^2) - 8a^3k_1(1-k_4)(k_2 - k_3)$$

$$k_1 = \sin a\cdot\sinh a; \quad k_2 = \sin a\cdot\cosh a$$

$$k_3 = \cos a\cdot\sinh a; \quad k_4 = \cos a\cdot\cosh a$$

$$a = (-Ra_\omega/4)^{1/4}.$$

NUMERICAL METHOD OF SOLUTION

Solutions of non-zero transpiration are solved by using a numerical method described in this section. The set of equations (14)–(16), is a sixth-order quasi-linear system with three boundary conditions at each end of the finite interval $0 \leqslant y \leqslant 1$. With the guessed values of missing boundary conditions at $y = 0$, i.e. $f''(0) = \alpha_1$, $f'''(0) = \alpha_2$ and $g'(0) = \alpha_3$, the boundary-value problem can then be converted to an initial-value one, and solved by using a fourth-order Runge–Kutta scheme. The values α_1, α_2 and α_3 are sought under the conditions of $f(1) = 1$, $f'(1) = 0$ and $g(1) = \delta$. The corrections $\Delta\alpha_i$'s can be obtained by a modified Newton's method [16] and, therefore, the initial guesses can be updated. The procedure is repeated until the criterion, $\max(\Delta\alpha_1, \Delta\alpha_2, \Delta\alpha_3) \leqslant 10^{-7}$ is satisfied.

In a preliminary numerical experiment, it is found that the integration procedure with a step size $\Delta y = 0.01$ is most pertinent and is adopted throughout the numerical computation. In the determination of the location of the flow reversal a step size $\Delta y = 0.005$ is used. The analytic solutions in the last section provide good initial guessed values for low-Re_w cases, and the calculations for the larger values of Re_w can be performed with the knowledge of the preceding cases. In the calculation, it is found that only a few iterations are needed to obtain a convergent solution. The number of iterations increases with the increase in the value of Re_w. The convergent solution can be easily obtained for $Re_w \leqslant 7$, but it is hard to get for $Re_w > 7$. This is attributed to the stiffness of the problem as Re_w increases. The solution can be obtained by introducing under-relaxation factors λ_i to the corrections of α_i, i.e. $\alpha_i + \lambda_i\Delta\alpha_i$.

RESULTS AND DISCUSSION

General features

Since air is considered as the coolant, a value of the Prandtl number of 0.7 is used in the present computations. Besides, there are four parameters, Ro, Ra_ω, Re_w and δ, involved in the problem. Among these parameters, the rotation number Ro characterizing the Coriolis effect was eliminated in the cross-differentiation of the x- and y-momentum equations. Physically, the Coriolis force, provides only the pressure distribution in this two-dimensional channel. The main flow Reynolds number is absorbed into the similarity variables and will not be presented explicitly. The rotational Rayleigh number Ra_ω, plays a very significant role in the problem. The magnitude of Ra_ω depends mainly on the rotational speed and the wall-temperature gradient τ; and the sign of Ra_ω depends on the type of buoyancy-assisted or buoyancy-opposed mixed convection. The asymmetry of the flow and temperature fields can be induced by the wall-transpiration and asymmetric wall-heating condition. The two sources of asymmetry are characterized by Re_w and δ, respectively.

Velocity and temperature distributions

Under the conditions of zero transpiration $Re_w = 0$ and symmetric wall heating $\delta = 0$, the flow and temperature fields in the channel are symmetric as shown in Fig. 2. The velocity and temperature distributions can be changed by the centrifugal force along the channel axis. The fluid near the hot walls is heated and retarded by the centrifugal-buoyancy force for $Ra_\omega > 0$, therefore, the velocity profiles near the channel axis must be extruded to satisfy the global continuity. The velocity profiles are distorted continuously with the increasing Ra_ω. As $Ra_\omega = 500.6$, the wall shear becomes zero. It is a critical value for the threshold of the flow reversal which occurred at the walls. On the contrary, in the case of $Ra_\omega < 0$, the velocity near the walls increases and the velocity profile near the channel axis is flattened. The flow velocity at the centre of the channel reduces to zero as $Ra_\omega = -6234$. This is a critical value for the in-field flow reversal. From Fig. 2(b), it is evident that the temperature solution can also be altered by the buoyancy effect. The larger the local velocity is, the cooler the fluid is.

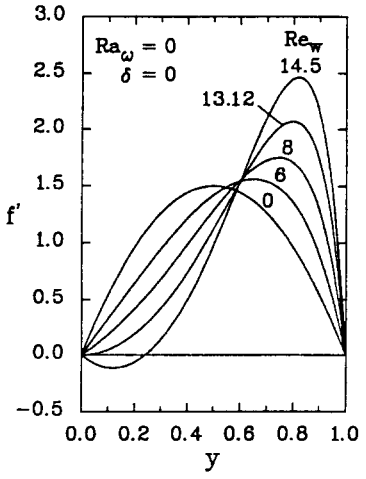

FIG. 3. Forced flow solution of semiporous channel flow.

In the case of pure forced convection, $Ra_\omega = 0$, equations (14) and (15) are decoupled and the equation of motion (14) is reduced to the so-called Berman equation. The solution is shown in Fig. 3. The peak velocity shifts toward the porous wall due to the wall suction. The local velocity in the channel remains non-negative until a critical Re_w is reached. The critical Re_w for the flow reversal in the SPC is 13.12.

Figure 4 shows a typical case of the buoyancy-assisted flow with an asymmetric wall heating,

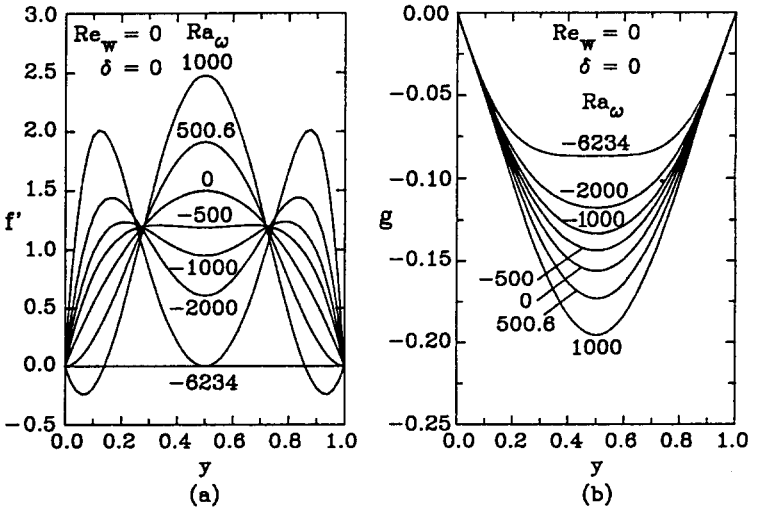

FIG. 2. Symmetric flow and temperature fields with $Re_w = \delta = 0$.

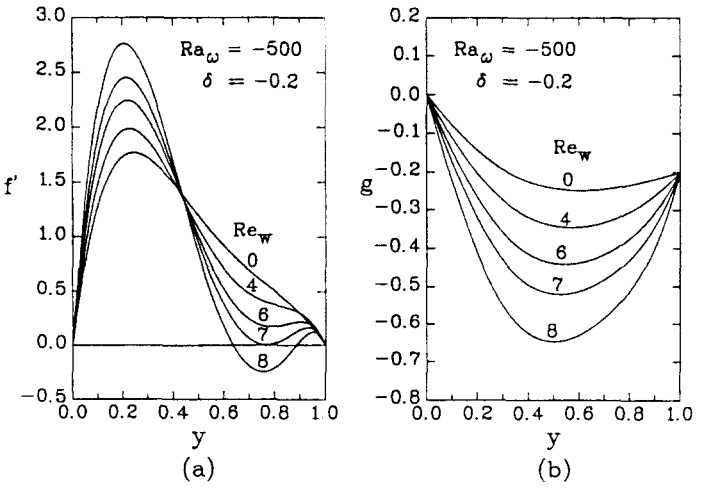

FIG. 4. Combined effect of suction and buoyancy in the cases of mixed convection with asymmetric wall heating.

$Ra_\omega = -500$ and $\delta = -0.2$, in which a behaviour caused by the coupled effect of wall suction and centrifugal buoyancy is revealed. The wall and fluid temperature difference, in the present SPC flow, is increased by the suction effect as shown in Fig. 4(b), and the buoyancy effect is augmented. The fluid near the walls can thus be further accelerated by the extra buoyancy force and a double-peak velocity profile can be generated. This is different from the one shown in Fig. 3.

Figure 5 shows the velocity and temperature distributions for the cases of flow reversal free (FRF) for a suction rate $Re_w = 5$ with various buoyancy and wall-heating conditions. For a highly asymmetric wall heating $\delta = 0.5$ or -0.5, the flow-reversal-free region is very narrow, e.g. $-138.0 \leqslant Ra_\omega \leqslant 132.9$ in Fig. 5(a), the velocity profiles are not much distorted from that of $Ra_\omega = 0$. For small values of δ, from Figs. 5(b) and (f), the velocity profiles still present a slight variation for the cases of $Ra_\omega > 0$. But in the cases of buoyancy-assisted mixed convection $Ra_\omega < 0$, highly distorted double-peak profiles result. The larger peak occurs near the hotter wall due to the buoyancy assisting effect. It is seen from Fig. 5(d) that, the asymmetry of the flow field arises simply from the wall transpiration. From the general view of Figs. 5(a)–(g), the temperature profiles are not so sensitive to the buoyancy effect as the velocity ones.

Flow and heat transfer parameters

The typical variations of the skin friction, pressure drop and heat transfer rate are shown in Figs. 6–8. The buoyancy-assisting effect, in general, may enhance the heat transfer but with the attendant penalty of high friction and pressure loss. On the contrary, the buoyancy-opposing effect reduces the skin friction and pressure drop as well as the heat transfer rate. The present prediction of centrifugal-buoyancy effects confirms the argument and experimental results proposed by Morris [14], and Harasgama and Morris [17].

Table 1. Nusselt number singularity in the case of asymmetric wall heating: $Re_w = 2$ and $\delta = 0.2$

Ra_ω	Nu_{w_∞}	Nu_{b_∞}	Nu
209.3	5.240	3.660	8.901
0	6.974	4.112	11.09
−200	9.959	4.521	14.48
−400	17.46	4.899	22.36
−600	85.04	5.244	90.28
−610	106.6	5.260	111.9
−630	218.0	5.293	223.3
−640	460.5	5.309	465.8
−649†	→ −∞	5.323	→ −∞
−660	−370.5	5.341	−365.2
−680	−131.2	5.373	−125.8
−800	−25.99	5.558	−20.43
−1000	−10.38	5.844	−4.539
−1500	−3.264	6.458	3.194
−1896	−1.568	6.866	5.298

† Singularity due to $T_w - T_b = 0$.

In some cases of asymmetric wall heating $\delta \neq 0$, the singularity in the Nusselt number may appear like that shown in Table 1. It is attributed to the situation of $T_w - T_b = 0$ and it will not destroy the validity and usefulness of the Nusselt number [18].

Flow reversal and critical conditions

In the present rotating SPC, the flow reversal can be induced by the centrifugal buoyancy and wall suction. Two modes, namely wall flow reversal (WFR) and in-field flow reversal (IFR), are presented.

In the symmetric flow ($Re_w = \delta = 0$) as shown in Fig. 2, it is seen that the flow is reversed near the wall $y = 0$ due to the buoyancy-opposing effect, but reversed at the channel axis due to the buoyancy-assisting effect. The pure suction effect tends to separate the flow near the solid wall as seen in Fig. 3. Nevertheless, if the buoyancy and suction are both

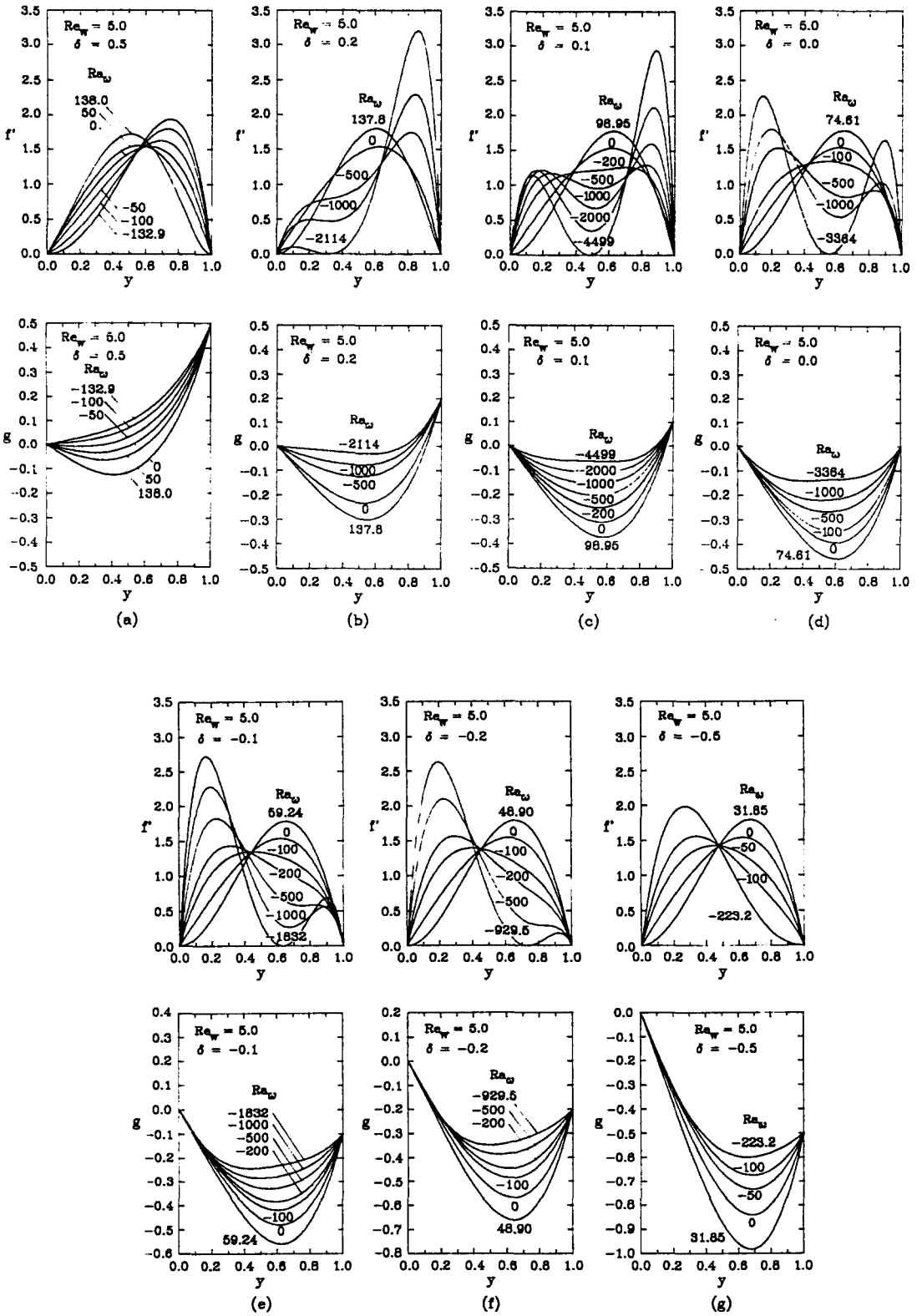

FIG. 5. Flow-reversal-free solutions of mixed convection with fixed suction rate $Re_w = 5$.

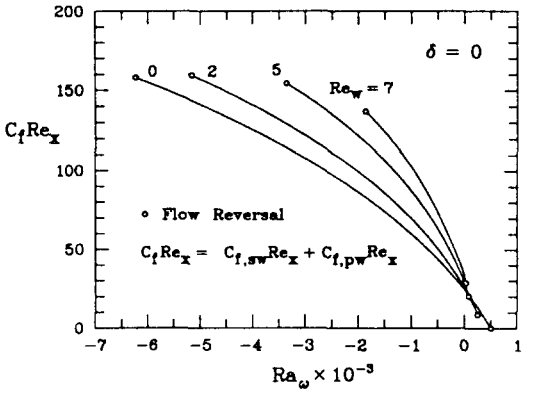

FIG. 6. Skin friction in the cases of symmetric wall heating.

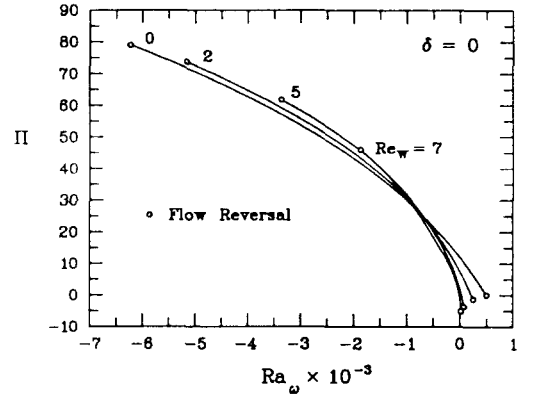

FIG. 7. Pressure drop in the cases of symmetric wall heating.

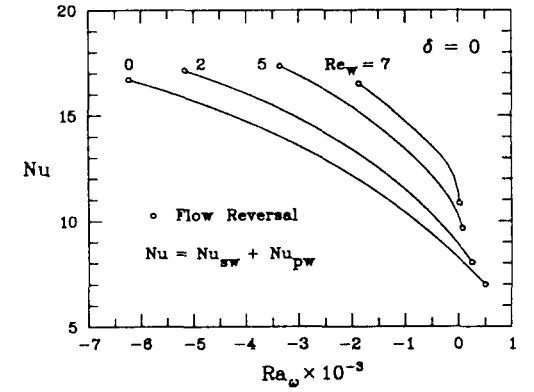

FIG. 8. Heat transfer rate in the cases of symmetric wall heating.

considered, the flow-reversal mechanism becomes coupled and complicated. The IFR, in Fig. 4, induced by the wall suction under the thermal influence is distinct from the WFR mode presented in Fig. 3 without the thermal effect.

Table 2 lists the critical Rayleigh number $Ra_{\omega,cr}$ and the location y_{cr} where the flow reversal occurs. Figures 9 and 10 are the corresponding flow-reversal parameter maps. Figure 9 shows the critical margin and the FRF regime. For a given Re_w, the bounding curve of the FRF region consists of a cusp in the buoyancy-opposed flow regime ($Ra_\omega > 0$), and a floral receptacle-like part in the buoyancy-assisted flow regime ($Ra_\omega < 0$). The general feature of this map is illustrated as follows by using the curves of $Re_w = 0$ as a typical example.

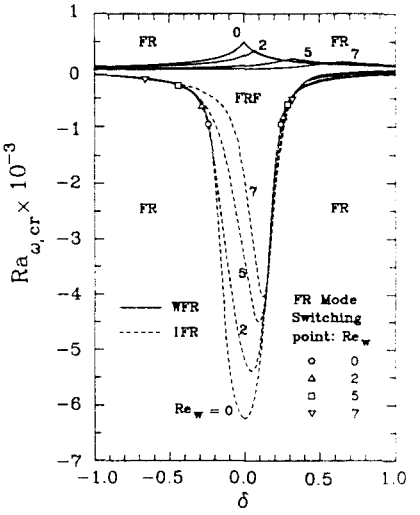

FIG. 9. Critical parameter map for flow reversal in the rotating SPC: FR, flow reversal; FRF, flow reversal free.

For $Re_w = 0$, the FRF region is symmetric and a cusp is located at $\delta = 0$. The flow reversal occurs at both walls simultaneously. The left and right curves to the cusp are critical boundaries corresponding to the flow reversal at solid and porous walls, respectively. Anyway, only the WFR mode appears in this buoyancy-opposed flow regime. In the buoyancy-assisted flow, however, either the WFR or the IFR mode is possible and its occurrence depends on the thermal boundary condition, i.e. the value of δ. The effect of δ on the flow-reversal location can be found in Fig. 10. In the zero-transpiration case, the IFR

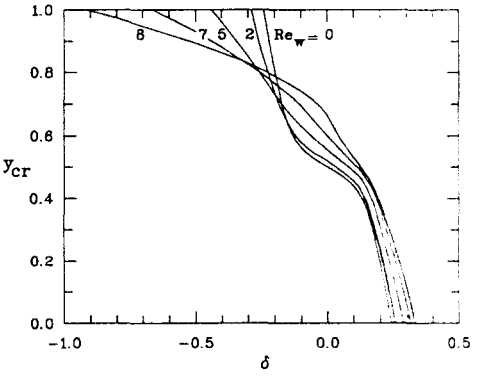

FIG. 10. Flow-reversal location in the cases of buoyancy-assisted mixed convection in the rotating SPC.

Table 2. Critical conditions for the flow reversal

	$Re_w = 0$				$Re_w = 2$			
	Opposed		Assisted		Opposed		Assisted	
δ	$Ra_{\omega,cr}$	y_{cr}	$Ra_{\omega,cr}$	y_{cr}	$Ra_{\omega,cr}$	y_{cr}	$Ra_{\omega,cr}$	y_{cr}
1.0	62.28	1.000	−85.57	0.000	68.89	1.000	−68.18	0.000
0.8	75.34	1.000	−112.2	0.000	76.13	1.000	−90.96	0.000
0.5	109.9	1.000	−212.0	0.000	111.4	1.000	−181.6	0.000
0.3	158.6	1.000	−527.1	0.000	161.6	1.000	−515.3	0.000
0.2	204.0	1.000	−1175	0.194	209.3	1.000	−1896	0.245
0.1	287.2	1.000	−5308	0.437	299.5	1.000	−5032	0.455
0.0	500.6†	1 and 0	−6234	0.500	249.1	0.000	−5166	0.520
−0.1	287.2	0.000	−5308	0.563	173.1	0.000	−3723	0.580
−0.2	204.0	0.000	−1175	0.806	131.9	0.000	−1614	0.735
−0.3	158.6	0.000	−527.1	1.000	106.3	0.000	−560.4	1.000
−0.5	109.9	0.000	−212.0	1.000	76.53	0.000	−214.8	1.000
−0.8	75.34	0.000	−112.2	1.000	53.82	0.000	−113.1	1.000
−1.0	62.28	0.000	−85.57	1.000	44.92	0.000	−86.11	1.000
	$Re_w = 5$				$Re_w = 7$			
	Opposed		Assisted		Opposed		Assisted	
δ	$Ra_{\omega,cr}$	y_{cr}	$Ra_{\omega,cr}$	y_{cr}	$Ra_{\omega,cr}$	y_{cr}	$Ra_{\omega,cr}$	y_{cr}
1.0	73.76	1.000	−39.40	0.000	90.19	1.000	−17.38	0.000
0.8	90.49	1.000	−55.32	0.000	176.0	1.000	−26.74	0.000
0.5	138.0	1.000	−132.89	0.000	102.4	0.000	−96.39	0.000
0.3	191.8	0.000	−541.3	0.315	46.08	0.000	−607.0	0.365
0.2	137.8	0.000	−2114	0.315	32.69	0.000	−2291	0.365
0.1	98.85	0.000	−4498	0.485	24.88	0.000	−3891	0.510
0.0	74.61	0.000	−3363	0.555	19.95	0.000	−1871	0.600
−0.1	59.24	0.000	−1832	0.630	16.60	0.000	−825.4	0.695
−0.2	48.90	0.000	−929.5	0.730	14.20	0.000	−502.3	0.765
−0.3	41.54	0.000	−512.5	0.850	12.39	0.000	−352.1	0.825
−0.5	31.85	0.000	−223.2	1.000	9.869	0.000	−206.8	0.930
−0.8	23.54	0.000	−119.8	1.000	7.552	0.000	−119.1	1.000
−1.0	20.05	0.000	−92.02	1.000	6.528	0.000	−92.88	1.000

† −501 [19]; −507 [3] in gravitational field.

mode appears at $|\delta| \leqslant 0.2407$, beyond this regime the flow reversal is switched to the WFR mode.

The presence of wall suction destroys the symmetry of the curves as well as narrows the FRF region. In the region of $Ra_\omega > 0$, the cusp is shifted toward positive δ. That means, to balance the suction effect on the solid wall, the double WFR is possible only when the porous wall is hotter than the solid wall. Since the combined effects of suction and buoyancy, in the case of $Ra_\omega < 0$, tends to generate the double-peak velocity profiles, the IFR mode can occur in a wide range of δ as seen in Fig. 10. It is noted that the asymmetric wall heating can always provide a premature condition for WFR, therefore, narrows the FRF region. In the cases studied, see Fig. 9, the FRF region shrinks to a narrow band as $|\delta| > 0.3$.

CONCLUDING REMARKS

In this paper, the mixed convection including the threshold of the flow-reversal phenomena in radially rotating SPC have been investigated over a wide range of parameters. The results provided a theoretical basis to understand the physics of this complex flow field.

The centrifugal buoyancy presents a salient influence on the hydrodynamic and thermal characteristics. This confirms the significance of the centrifugal-buoyancy effect on the flow and heat transfer in the rotating thermal systems. In radially outward flow $Ra_\omega > 0$, the centrifugal-buoyancy effect reduces the heat transfer rate; but in the radially inward flow $Ra_\omega < 0$, the heat transfer can be enhanced by this effect.

The wall-suction effect is beneficial to the heat transfer performance of the transpiration cooling as expected. The wall suction, like the buoyancy-opposing effect, may also induce flow reversal. If both the suction and buoyancy are considered, the combined effect on the flow field and therefore the flow-reversal mode is very distinct from that of pure suction.

Both the wall-suction and buoyancy-opposing effect may induce flow reversal and thus destabilize the flow field in the channel. Two maps of the critical conditions have been developed; and they may give a

clear insight into this critical phenomenon. However, flow reversal in fully-developed channel flow is still a controversial and paradoxical subject. More theoretical studies, e.g. stability analysis, are required to attain a comprehensive understanding of the flow structure.

REFERENCES

1. A. S. Berman, Laminar flow in channels with porous walls, *J. Appl. Phys.* **24**, 1232–1235 (1953).
2. S. W. Yuan and A. B. Finkelstein, Laminar pipe flow with injection and suction through a porous wall, *ASME Trans.* **88**, 719–724 (1956).
3. L. F. Carter and W. N. Gill, Asymptotic solution for combined free and forced convection in vertical and horizontal conduits with uniform suction and blowing, *A.I.Ch.E. Jl* **10**, 330–339 (1964).
4. R. B. Kinney, Fully developed friction and heat transfer characteristics of laminar flow in porous tubes, *Int. J. Heat Mass Transfer* **11**, 1393–1401 (1968).
5. R. M. Terrill, Heat transfer in laminar flow between parallel porous plates, *Int. J. Heat Mass Transfer* **8**, 1491–1497 (1965).
6. G. Raithby, Laminar heat transfer in the thermal entrance region of circular tubes and two-dimensional rectangular ducts with wall suction and injection, *Int. J. Heat Mass Transfer* **14**, 224–243 (1971).
7. P. L. Donoughe, Analysis of laminar incompressible flow in semi-porous channels, NASA TN 3759, NACA (1956).
8. E. R. G. Eckert, P. L. Donoughe and B. J. Moore, Velocity and friction of laminar viscous boundary-layer and channel flow over surfaces with ejection or suction, NASA TN 4102, NACA (1957).
9. S. J. Rhee and D. K. Edwards, Laminar entrance flow in a flat plate duct with asymmetric suction and heating, *Numer. Heat Transfer* **4**, 85–100 (1981).
10. M. M. Sorour and M. A. Hassab, Effect of sucking the hot fluid film on the performance of flat plate solar energy collectors, *Appl. Energy* **14**, 161–173 (1983).
11. M. M. Sorour, M. A. Hassab and S. Estafanous, Developing laminar flow in a semiporous two-dimensional channel with nonuniform transpiration, *Int. J. Heat Fluid Flow* **8**, 44–54 (1987).
12. S. L. Moskowitz and S. Lombardo, 2750 Deg F engine test of a transpiration air-cooled turbine, *ASME Trans., J. Engng Pwr* **93**, 238–248 (1971).
13. R. Raj, Deposition results of a transpiration air-cooled turbine vane cascade in a contaminated gas stream, *ASME Trans., J. Engng Pwr* **105**, 826–833 (1983).
14. W. D. Morris, *Heat Transfer and Fluid Flow in Rotating Coolant Channels*. Wiley, Chichester (1981).
15. R. Siegel, Analysis of buoyancy effect on fully developed laminar heat transfer in a rotating tube, *ASME Trans., J. Heat Transfer* **105**, 338–344 (1985).
16. M. Rahman, On the numerical solution of the flow between a rotating and a stationary disk, *J. Comp. Appl. Math.* **4**, 289–293 (1978).
17. S. P. Harasgama and W. D. Morris, The influence of rotation on the heat transfer characteristics of circular, triangular, and square-sectioned coolant passages of gas turbine rotor blades, *ASME Trans., J. Turbomachinery* **110**, 44–50 (1988).
18. W. M. Kays and M. Crawford, *Convective Heat and Mass Transfer* (2nd Edn), pp. 100–101. McGraw-Hill, New York (1980).
19. S. Ostrach, Combined natural and forced-convection laminar flows and heat transfer in fluids with and without heat sources in channels with linearly varying wall temperatures, NASA TN 3141, NACA (1954).

CONVECTION MIXTE LAMINAIRE DANS UN CANAL SEMI-POREUX TOURNANT RADIALEMENT

Résumé—On étudie les caractéristiques d'écoulement et de transfert thermique de la convection laminaire dans un canal semi-poreux tournant radialement avec une transpiration uniforme et un gradient de température constant à la paroi. L'effet de flottement est pris en compte en considérant la variation de densité dans le terme de force centrifuge. On suppose une solution affine: les effets de rotation, de transpiration et de chauffage pariétal sur les champs de vitesse et de température, le frottement à la paroi, la perte de pression et le flux thermique sont analysés dans la solution de deux équations couplées quasilinéaires. Des phénomènes d'écoulement de retour peuvent être créés par la transpiration et le flottement. Deux modes de retour d'écoulement et les conditions critiques associées sont étudiés en détail pour explorer le mécanisme de la convection mixte.

LAMINARE MISCH-KONVEKTION IN EINEM UM SEINE ACHSE ROTIERENDEN HALBPORÖSEN KANAL

Zusammenfassung—Strömung und Wärmeübergang bei laminarer Misch-Konvektion in einem um seine Achse rotierenden halbporösen Kanal werden für den Fall gleichförmiger Transpiration und konstanter Temperaturgradienten an der Wand untersucht. Auftriebseffekte werden durch eine Dichtevariation im Term für die Zentrifugalkraft berücksichtigt. Durch Lösen der beiden gekoppelten quasilinearen Gleichungen werden die Einflüsse der Rotation, der Transpiration un der Beheizung der Wand auf die Geschwindigkeits- und Temperaturfelder, die Schubspannung, den Druckabfall und Wärmeübergang untersucht. Rückströmerscheinungen können durch Transpirations- und Auftriebseffekte verursacht werden. Zwei Arten der Rückströmung und die damit verbundenen kritischen Zustände werden detailliert untersucht, um den Mechanismus der Mischkonvektion zu erforschen.

ЛАМИНАРНАЯ СМЕШАННАЯ КОНВЕКЦИЯ В РАДИАЛЬНО ВРАЩАЮЩЕМСЯ КАНАЛЕ ИЗ ПОРИСТОГО МАТЕРИАЛА

Аннотация—Исследуются динамические и тепловые характеристики ламинарной смешанной конвекции в радиально вращающемся канале из пористого материала с однородным испарением и постоянным градиентом температур на стенке. Действие подъемной силы учитывается величиной, описывающей изменение плотности. На основе полученного автомодельного решения исследуется влияние вращения, испарения и нагрева стенки на поля скоростей и температур, поверхностное трение, перепад давления и скорость теплопереноса путем решения двух взаимосвязанных квазилинейных уравнений. Эффектами испарения и подъемной сили могут вызываться явления обращения течения. С целью изучения механизмов смешанной конвекции подробно рассматриваются две модели обращения течения и соответствующие критические условия.